High efficiency echelle gratings for MIGHTI, the spatial heterodyne interferometers for the ICON mission

Christoph R. Englert[1], Charles M. Brown[1,*], Bernhard Bach[2], Erich Bach[2], Kirk Bach[2], John M. Harlander[3,4], John F. Seely[4], Kenneth D. Marr[1], Ian Miller[5]

[1] *Naval Research Laboratory, 4555 Overlook Ave. SW., Washington, D.C. 20375*
[2] *Bach Research Corp., 4946 63rd St., Boulder, CO 80301*
[3] *St. Cloud State University, 720 4th Avenue South, St. Cloud, MN 56301*
[4] *Space Systems Research Corporation, 1940 Duke Street, Alexandria, VA 22314*
[5] *LightMachinery, Inc., 80 Colonnade Road North, Unit #1, Ottawa, ON K2E 7L2, Canada*
**Corresponding author: charles.brown@nrl.navy.mil*

Received 11 November, 2016; revised 31 January, 2017; accepted XX Month XXXX; posted XX Month XXXX (Doc. ID XXXXX); published XX Month XXXX

Development of a new generation of low groove density blazed echelle gratings optimized for MIGHTI, a space borne spatial heterodyne interferometer operating in the visible and near infrared is described. Special demands are placed on the wavefront accuracy, groove profile, and efficiency of these gratings. These demands required a new ruling for this application with significant improvements over existing gratings. Properties of a new generation of highly efficient, plane gratings with 64 grooves/mm blazed at 8.2° are reported.

OCIS codes: (050.1950) Diffraction gratings; (300.6300) Spectroscopy, Fourier transform; (010.1330) Atmospheric turbulence; (120.6200) Spectrometers and spectroscopic instrumentation

http://dx.doi/org/10.1364/AO.99.09999

1. INTRODUCTION

The Ionospheric Connection Explorer (ICON) project is a NASA sponsored Explorer class satellite mission. It aims to explore the boundary between Earth and space by probing the extreme variability of Earth's ionosphere with *in-situ* and remote-sensing instruments. A principal instrument on ICON is the Michelson Interferometer for Global High-resolution Thermospheric Imaging (MIGHTI) built at the Naval Research Laboratory and tasked to remotely measure the neutral wind field and temperatures at altitudes between 90 and 300 km [1].

The MIGHTI instrument uses the Doppler shift of the naturally occurring atomic oxygen red (630.0nm) and green (557.7nm) lines to measure wind velocities. The temperature in the lower thermosphere is derived from the spectral shape of the molecular oxygen A band around 760nm [2, 3], which is sampled by narrow band interference filters at the MIGHTI array detectors. The wind vectors are derived by making two perpendicular line of sight wind speed measurements 45° and 135° in azimuth from the satellite ram direction. MIGHTI uses two identical field widened Michelson interferometers and uses the fringe phase shifts resulting from the Doppler shifts of the emission lines to derive the line of sight wind velocities. This concept is fundamentally similar to the technique employed by the highly successful WINDII instrument on UARS [4], which used an interferometer with a movable mirror in one interferometer arm to sample several phase points of a monochromatic fringe.

MIGHTI uses a modified Spatial Heterodyne Spectroscopy (SHS) technique called Doppler Asymmetric Spatial Heterodyne (DASH) spectroscopy, which eliminates moving interferometer parts by replacing the interferometer mirrors with fixed tilted gratings and which produces an interferogram around the optical path difference for which the Doppler shift sensitivity is the largest [5-10]. One can think of the individual grating facets as small mirrors, all at different optical path differences, that are imaged on the array detector, where many dozens of optical path difference samples of the interferogram are recorded simultaneously. Figures 1 and 2 give schematics of the DASH interferometer .

The DASH technique provides several advantages, including the monolithic design and the ability to simultaneously observe a

calibration line. However other instrument aspects have to be addressed so they do not outweigh the advantages. The main challenge of the field widened DASH interferometer is the lower efficiency compared to a classical Michelson interferometer with flat, rooftop or corner cube mirrors, for which the absolute efficiency is typically determined by the reflectivity of the mirror surface coatings and beamsplitter efficiency only. The absolute efficiency of gratings on the other hand is not only determined by the coating reflectivity, but also by other parameters including the effective area that is lost to the backsides of the facets, the blaze angle, the facet flatness, the angular beam shape and the overall beam angle.

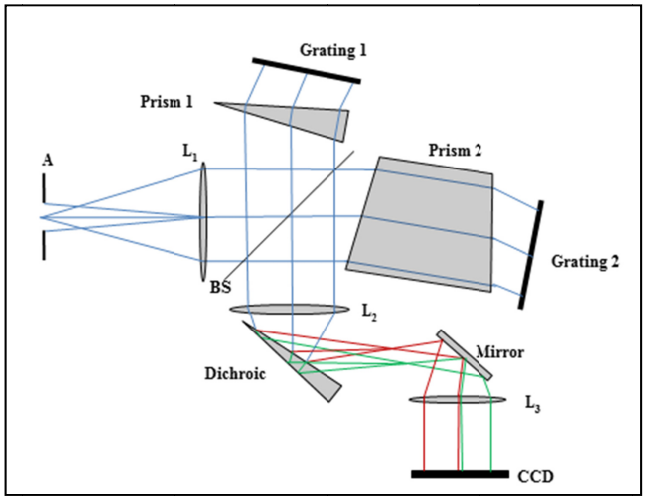

Figure 1. Schematic of a DASH interferometer for MIGHTI. Light from the sky enters from the left and is imaged onto two identical gratings at the ends of the beamsplitter (BS) arms. Diffracted light passes back through the arms to the beamsplitter where it recombines and the resulting interference fringes are imaged on an array detector such as a CCD (Charge Coupled Device). A Dichroic prism in the output optics separates the green 557nm light from the red and infrared light.

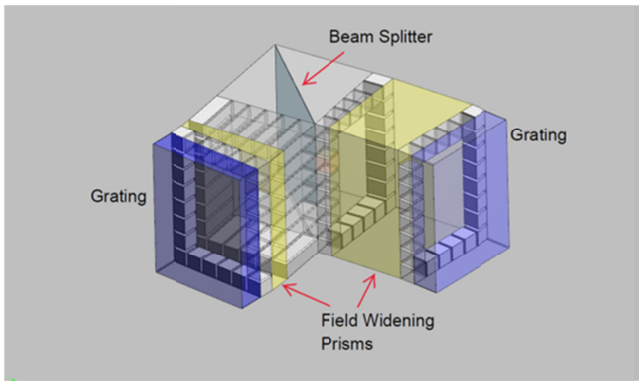

Figure 2. 3D schematic of the MIGHTI DASH interferometer. The non-polarizing N-Bk7 beamsplitter is ~50% transmitting/reflecting. The field widening prisms are of SF57 glass and are attached to the cube by angled spacer blocks. The gratings are on fused silica blanks and are attached to the field widening prisms by fixed plane parallel spacer blocks. By using the spacer blocks, we avoid having additional glass in the light path and allow for the thermal mismatch between the different optical glasses used [11].

2. GRATING REQUIREMENTS

Since MIGHTI is operating at 630.0nm, 557.7nm and around 760nm, the MIGHTI gratings require high efficiency at all of these wavelengths. The oxygen red line is the most challenging measurement, especially at the bottom side of its nighttime airglow layer where the atmospheric signal is weak, which is why the MIGHTI gratings have been optimized for 630.0nm rather than for 557.7nm or 760.0nm. The bright O_2 band at 760 nm is used to determine atmospheric temperatures using the band's rotational structure, which is sampled with narrow interference filters at the detector without the need for resolving DASH fringes.

Planning of the experiment showed that all of the above wavelengths and mission requirements could be achieved by building an interferometer with high efficiency plane gratings with a groove density of 64 l/mm operating on blaze in 8th order for the green line, 7th order for the red line, and 6th order for the molecular oxygen band in the near infrared.

To meet the ICON science requirements, the grating requirements of MIGHTI exceeded the specifications of any commercially available grating, so an effort was made to construct the necessary gratings. This paper presents the details of producing and evaluating two generations of gratings to achieve our goals. Table 1 summarizes the specifications for the MIGHTI gratings, as negotiated with grating vendors to be within state-of-the art capabilities.

Table 1. MIGHTI Grating Specifications

Item	Detail
Wavelengths of interest	630nm, 558nm Interferometric 750 – 780nm Signal only
Substrate	Fused silica, 42 x 32.3 mm x 8mm. Grating substrates polished flat and square on all sides.
Ruling	Central 29 x 18 mm of front face, leaving an outer bare fused silica zone for bonding grating to the interferometer. Grooves parallel to long edge of substrate to better than 5.0 arc min
Groove density	64.285 lines/mm
Blaze angle	8.2 degrees nominal, blazed for 558nm (8th order), 630nm (7th order), and 760nm (6th order)
Efficiency	Following best practices, optimized for 7th and 8th orders
Diffracted wavefront	Flat to λ/10 wave at 558nm
Grating coating	Gold
Parallelism between blank and grating surface	Following best practice

The grating blanks were fused silica and were specified to be flat, with the side faces polished flat and perpendicular to the front face and to each other. The side faces were used as a reference for aligning the grating grooves and for orienting the gratings when assembling the interferometer. In addition, on the front face a clear 5 mm wide border (Fig. 3) was left outside the grating rulings to permit bonding the gratings to the interferometer arms. Conventional gratings ruled in gold were

indicated to allow blazing for maximum efficiency at 630nm. As DASH uses the gratings in the Littrow configuration, a triangular groove profile with a blaze angle of 8.2° was specified.

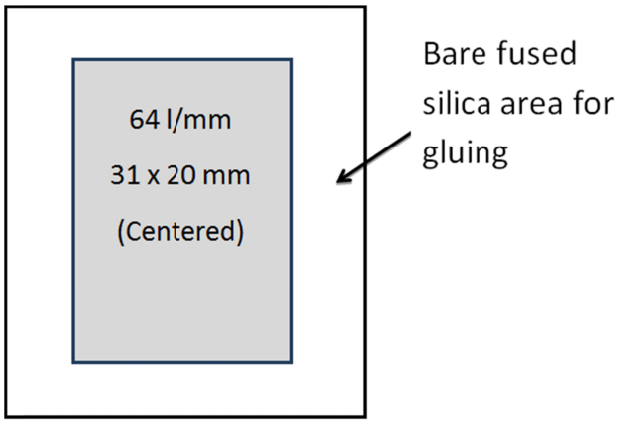

Figure 3. Diffraction grating blank and ruled area – schematic. Grating blank is 42 mm x 32.2mm.

Two additional requirements arise from the interferometer application: first, the diffracted wavefronts from the two gratings need to be flat within ~1/10 wave to keep the fringes straight, and second, the grooves of the two gratings need to be aligned such that the grating dispersions are in the same plane. The first requirement is managed by ruling on a flat substrate and by careful replication technique. The second is managed by using a side face as a reference for the direction of the ruling engine. Knowledge of the master ruling direction is 1 arc min or better. Thereafter, the side faces are used to orient a grating blank and master parallel to each other during replication. This was accomplished by using a replication fixture to hold the master grating and product substrate, maintaining alignment while the epoxy cures. To achieve the precision needed for the MIGHTI gratings, the working surfaces of the fixture were ground to achieve the needed planarity, the polished substrate sides were the reference surface and micrometers were used for incremental adjustments. Once the master and replica substrates were mated in the fixture, the return image of an autocollimator was used to align the reference surfaces. The whole apparatus was then subject to the curing cycle. Once the epoxy cured, the replica "sandwich" was transferred to a standard fixture used to separate the master from the product. The side and bottom faces of the replica gratings are subsequently used as reference surfaces for aligning the grooves when assembling the SHS interferometers.

3. GRATING EFFICIENCY

The absolute grating efficiency is limited by several factors including: reflectivity of the coating, facet angle, backside facet angle, and facet surface quality, which is important for minimizing scattering, ghosts, and unwanted orders. A gold coating was selected as it has, among suitable materials, the best reflectivity at 630nm (≈93%), the wavelength of the weakest thermospheric emission line of interest. Moreover, it shows acceptable reflectivity for the green line and the molecular oxygen band. Likewise, the facet angle was selected to put 630.0nm on blaze. By choosing 7th order for 630nm, the other wavelengths, 557nm and 760nm, are also on blaze in 8th and 6th orders, respectively. The steepest practical backside angle is sought as light striking this side of the grooves is lost into high negative orders. The steepness of the backside angle is limited by the ruling process and by the difficulty it imposes on the separation of replicas from the master during processing. The roughness of the grating facets and edges and irregularity of grooves all contribute to light losses through scattering and grating ghosts.

The ideal efficiency was calculated using the PCGrate simulation code [12] (described below) of an ideal gold-coated grating having perfectly flat and smooth blazed groove facets at 8.2° angle, 90° peak corner angle, and 81.8° opposite facet angle. In this ideal case the efficiencies would be 93%, 90%, and 75% in the 6th order at 760 nm, 7th order at 630 nm, and 8th order at 558 nm, respectively. These values represent the theoretical limit of what is achievable.

On this basis, a prototype grating was ruled and two replicas produced. These replicas were measured, tested, and assembled into a prototype interferometer block. While meeting the nominal specifications stated in Table 1, these gratings only produced an efficiency of ~50% at 630nm. PCGrate simulations using the groove profile measured by atomic force microscopy (AFM) showed that it was likely that a more efficient grating could be produced by improving the facet roughness and the groove shape, directly resulting in a significant improvement of the MIGHTI performance.

After additional experimentation with ruling stylus shape and pressure, gold thickness and deposition, a second grating master was produced. This grating had smoother facets and a steeper backside angle. Eight fourth generation replicas of this master have been produced for the MIGHTI flight instrument (FM-*n*), for an engineering model (EM-*n*), and for two flight spares. In the following sections, the measurements and properties of these flight gratings, which are all replicas of the same master, are presented.

4. GRATING SURFACE PROFILES AND GROOVE MODELING

After the replicas were produced, AFM measurements of the groove profiles were made at Bach Research and at St. Cloud State University. Figure 4 shows the AFM profiles of an engineering model grating replicated from the final master ruling. The Flight Model (FM) gratings are also replicas of this master.

The efficiencies were modeled with the PCGrate code which solves Maxwell's equations for an electromagnetic wave incident on the grating groove and accounts for the measured irregular shape, the measured roughness of the groove profile, and the index of refraction of the coating and the grating substrate. The Fresnel reflectivity and transmissivity coefficients are calculated at each interface of the coating on the groove and at the underlying grating substrate. The code has proven to be accurate for a variety of master, replica, and multilayer coated gratings [13, 14]. The primary inputs to the code are the groove profile and the optical constants of the coating and the substrate. In the case of MIGHTI, the groove profile was measured by atomic force microscopy (AFM), and the optical constants were from Palik [15]. Since gold is opaque in the visible, only one interface was modeled, the top gold coating.

The EM-1 groove profile with a pristine gold coating was used to calculate the efficiency. The efficiency calculations were performed by setting the angle of incidence on the grating to the Littrow condition for 7th order and 632.8 nm wavelength

(assumed to be 8.16° for the calculations). For the measurements described below, the grating was also rotated by 0.4° out-of-plane so the detector could be scanned through the diffracted orders without occulting the incident beam. This angle was included in the calculations.

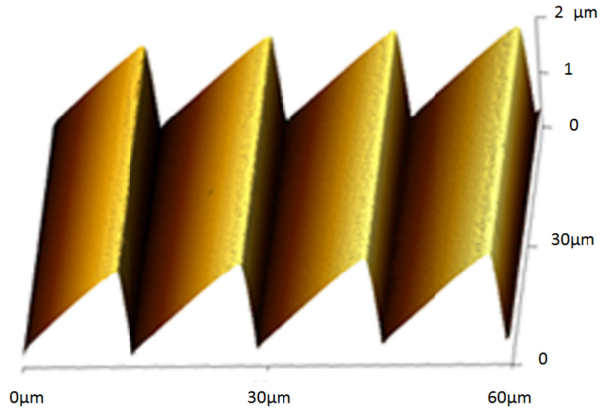

Figure 4. AFM image of MIGHTI grating grooves.

The groove model was constructed from AFM data considering the following information:

(a) The surface data of EM-1 shown in Figure 5 was corrected for leveling by adding an angle of 0.059°.
(b) Quadratic curves are fit to the blaze facet and the backside facet.
(c) The standard deviation from the quadratic curves is ± 7.6 nm. Away from the rounded vertex and trough, the deviation from the smooth quadratic fitted to the working blaze facet is 4 nm.
(d) Average fitted angle on the blaze facet was 7.38°, and the backside facet angle (beyond the rounded vertex) varies from 20° to 60°. This AFM groove shape was input into the PCGrate code and the calculated efficiency was compared to 633nm measured efficiencies, which peak in the 7th order with values ranging from 70.0% to 73.4%.

Using the measured 7.38° blaze angle of the EM-1 groove, the calculated on-blaze order number is 6.3 and the efficiency at 632.8 nm wavelength is shared between the 6th and 7th orders and the calculated 632.8nm efficiencies were much lower than the measured efficiencies. To bring the calculations into agreement with observations, EM-1 groove height was increased by 10%, increasing the facet angle to 8.1°. With this one adjustment, practically all of the efficiency at 632.8 nm appears on blaze in the 7th order. While the AFM accurately measured the 180 nm depths of holes on a calibration sample, it apparently under-measured the much larger 1.73 µm grating groove depth by 10%. While the 70% calculated efficiency in the on-blaze 7th order is a few percent lower than the measured efficiencies, the calculated and measured efficiencies are otherwise in good agreement.

The AFM is an excellent tool with which to determine groove shape and roughness due to its ability to image features as small as a few angstroms. The hope that it could become the ultimate standard for predicting grating performance has not so far proven to be the case. Since it looks only at a ~100 micron area at a time, its results have to be verified by spectral measurements over a wider range to determine the actual blaze and groove depth achieved. With that information, one can manipulate the ruling diamond shape and weight to arrive at the desired blaze.

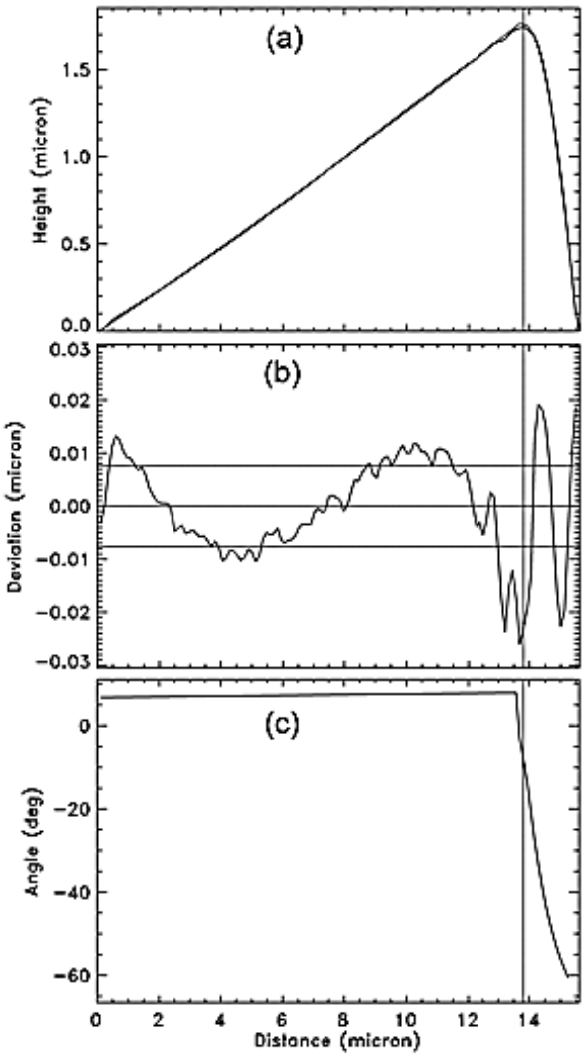

Figure 5. Groove profile derived from AFM scans of a replica from the FM master grating. Panel (a) is the measured profile and the fitted profile, which is almost identical, panel (b) is the deviation from a quadratic fit, and panel (c) is the facet angle across the groove.

5. GRATING EFFICIENCY MEASUREMENTS

Two sets of efficiency measurements were made, one, the "MIGHTI configuration" was made with a fixed angle of incidence as in the MIGHTI instrument, and the second "Littrow configuration" was made with a fixed detector and variable angle of incidence so that the

measurement was always made at the Littrow angle for the order in question.

Various unpolarized lasers operating at 632.8, 557.7 and 543nm were used to measure the grating efficiency in the red and green bands. Figure 6 shows a schematic of the measurement geometry. The lasers reflect from near the top edge of a mirror and onto the grating. In this "MIGHTI configuration", the grating is aligned to put 7th (red) or 8th (green) order at the Littrow condition for an angle of 8.2°. The grating was also tilted out of plane by 0.4° so diffracted rays can pass above the top edge of the mirror and are then measured with a power meter scanning the locations of the different orders. Incident laser power was measured by moving the power meter to the dashed location in Figure 6. Laser spots were 5-6mm in diameter at the grating and at the power meter, underfilling the 9.5mm diameter power meter by a comfortable margin.

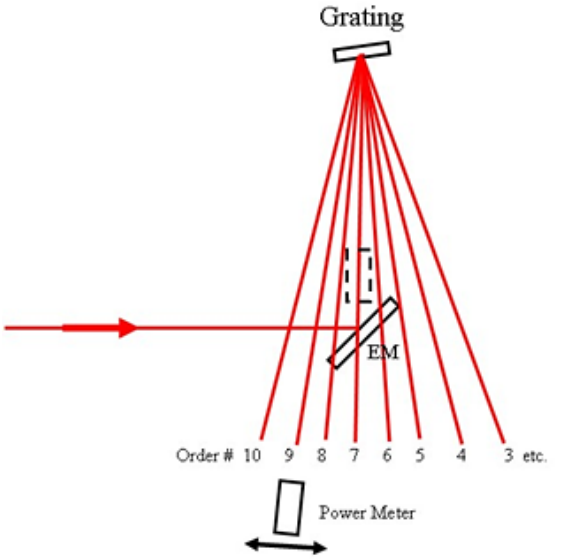

Figure 6. Schematic of arrangement for measuring grating efficiency in the MIGHTI configuration near 7th and 8th orders for the red and green sources, respectively. A 45° mirror used near its edge (EM) directs the laser beam to the grating. The angle of incidence was fixed at 8.2° and the power meter moved through the orders or to the dashed location to measure incident power.

The Littrow configuration was similar, except the power meter was stationary and the grating was rotated through many orders. Table 2 summarizes measured efficiencies of several of these sister replica gratings made with lasers near the working wavelengths of the gratings and in orders near the working orders.

Table 2. Efficiency measurements of several sister gratings in the MIGHTI configuration.

	Efficiency (%)									
	632.8 nm						543.4 nm			557.7 nm
Order	FM-4	FM-5	FM-6	FM-7*	EM-1	EM-2	FM-4	FM-5	FM-6	FM-7*
4				1.49	1.9	1.7				0.57
5				1.42	2.2	2.0				1.16
6	0.09	0.10	0.06	0.63	0.1	0.1				1.53
7	71.6	71.2	70.8	69.9	72.1	72.5	2.6	2.3	2.2	0.18
8	3.2	3.2	3.1	5.35	3.8	3.6	50.4	50.1	51.7	61.6
9				0.18	0.3	0.3	8.8	8.5	7.9	3.72
10				0.10	0.1	0.1				0.27

These values are not adjusted for the reflectivity of the gold coating, 93% at 632.8nm, 77% at 543nm, and 83.5% at 558nm [15]. *The FM-7 measurements were made with the frequency stabilized lasers as detailed below.

A. FM-7 Efficiency at 557.7nm, 632.8nm, MIGHTI configuration

The measurement geometry was as follows: Two frequency stabilized and polarized lasers operating at 557nm and 632.8nm were used to measure the FM-7 grating efficiency in wavelength bands of MIGHTI. The final setup is as in Figure 6, but a beamsplitter was introduced into the incident beam and a second power meter added to monitor the brightness of the lasers, which in the case of the green laser varied significantly with time. For the green laser, a solid state device, a collimating lens, a faraday rotator, and a narrow band filter were added to help eliminate back reflections into the laser and to eliminate an unwanted infra-red emission from the laser. The grating was aligned to put either 7th or 8th order at the Littrow angle (α = 8.2°). These lasers were aligned with their polarization at 45° to the grating grooves. By using the two channel power meter, the data were corrected for laser power variations. By logging the data with a computer, more than 100 individual readings were averaged for each data point. The accuracy achieved was better than 0.1% for all but the faintest orders. Table 3 and Figure 7 report measured efficiencies for all accessible orders of grating FM-7. Typical stray light levels observed between orders were less than 0.1% of the nearby orders.

Table 3. Measured Efficiency of Grating FM-7.

Order	Grating efficiency		Order	Grating efficiency	
	557.7nm	632.8nm		557.7nm	632.8nm
-23	7.60E-04		5	1.16E-02	1.42E-02
-22	2.00E-03		6	1.53E-02	6.33E-03
-21	1.80E-03		7	1.83E-03	6.99E-01
-20	1.51E-03	3.24E-03	8	6.16E-01	5.35E-02
-19	2.44E-03	1.92E-03	9	3.72E-02	1.76E-03
-18	3.58E-03	3.86E-03	10	2.75E-03	1.05E-03
-17	1.78E-03	3.97E-03	11	9.79E-04	1.43E-03
-16	2.44E-03	2.77E-03	12	1.12E-03	1.48E-03
-15	3.06E-03	4.99E-03	13	1.32E-03	9.84E-04
-14	1.96E-03	3.88E-03	14	9.34E-04	4.87E-04
-13	1.95E-03	2.15E-03	15	3.98E-04	2.77E-04
-12	1.01E-03	2.68E-03	16	1.41E-04	3.22E-04
-11	1.24E-03	3.40E-03	17	1.60E-04	3.90E-04
-10	1.77E-03	2.64E-03	18	2.35E-04	4.02E-04
-9	1.49E-03	1.50E-03	19	2.60E-04	3.33E-04
-8	7.05E-04	1.22E-03	20	2.11E-04	2.45E-04
-7	4.82E-04	1.77E-03	21	1.42E-04	1.81E-04
-6	9.55E-04	2.68E-03	22	9.95E-05	1.46E-04
-5	1.28E-03	3.19E-03	23	7.65E-05	1.33E-04
-4	1.31E-03	2.58E-03	24	6.87E-05	1.33E-04
-3	8.33E-04	1.21E-03	25	5.91E-05	1.26E-04
-2	3.07E-04	6.63E-04	26	4.82E-05	1.11E-04
-1	4.89E-04	1.65E-03	27	3.74E-05	9.07E-05
0	1.29E-03	3.16E-03	28	2.76E-05	7.15E-05
1	1.90E-03	4.38E-03	29	2.44E-05	
2	2.16E-03	6.05E-03	30	2.40E-05	
3	3.00E-03	9.54E-03	31	1.96E-05	
4	5.66E-03	1.49E-02			

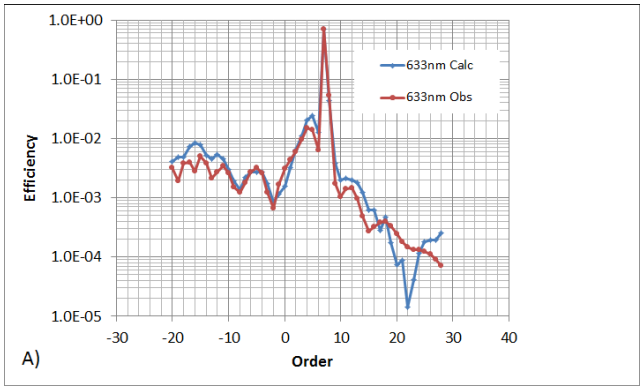

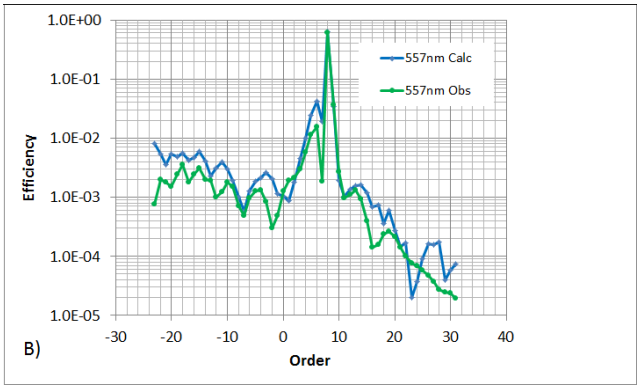

Figure 7. Measured and calculated efficiencies for grating FM-7 at a fixed 8.2° angle of incidence. Peak efficiency is in 7th order(A) at 633nm and 8th order (B) at 558nm.

B. FM-7 Efficiency at 632.8nm, Littrow configuration

A second detailed set of 633nm efficiency measurements (see Table 4) were made with the grating mounted on a rotary stage so it could be scanned through many orders in the Littrow configuration with a fixed detector. Measurements of this sort were made on FM-7 at NRL and on EM-1 at St. Cloud State University.

Table 4. Grating FM-7 efficiency at 632.8nm (unpolarized) in the Littrow configuration.

Order	Obs. Efficiency	Calc. Efficiency	Littrow angle (°)	Order	Obs. Efficiency	Calc. Efficiency	Littrow angle (°)
-48	5.13E-04		-77.5	0	3.25E-03	5.63E-04	0.0
-47	1.13E-03		-72.9	1	3.54E-03	2.78E-03	1.2
-46	5.31E-03		-69.3	2	4.35E-03	7.47E-03	2.3
-45	6.59E-03		-66.2	3	6.69E-03	1.45E-02	3.5
-44	1.73E-02		-63.5	4	1.02E-02	2.74E-02	4.7
-43	4.27E-02		-61.0	5	8.39E-03	3.70E-02	5.8
-42	5.63E-02		-58.7	6	8.97E-03	1.55E-02	7.0
-41	4.61E-02		-56.5	7	7.00E-01	6.74E-01	8.2
-40	2.40E-02		-54.4	8	6.37E-02	4.49E-02	9.4
-39	8.95E-03		-52.5	9	2.00E-03	1.90E-03	10.5
-38	4.58E-03		-50.6	10	1.45E-03	9.93E-04	11.7
-37	7.14E-03		-48.8	11	1.79E-03	1.30E-03	12.9
-36	7.11E-03		-47.1	12	1.69E-03	1.06E-03	14.1
-35	4.36E-03		-45.4	13	1.03E-03	9.61E-04	15.3
-34	1.27E-03		-43.8	14	4.25E-04	6.72E-04	16.5
-33	1.74E-03		-42.2	15	2.70E-04	2.59E-04	17.8
-32	2.91E-03		-40.6	16	3.60E-04	2.87E-04	19.0
-31	3.27E-03		-39.1	17	4.23E-04	1.79E-04	20.2
-30	2.46E-03		-37.6	18	3.53E-04	2.21E-04	21.5
-29	2.01E-03		-36.1	19	2.23E-04	7.71E-05	22.7
-28	1.14E-03		-34.7	20	1.28E-04	5.70E-05	24.0
-27	1.47E-03		-33.3	21	9.93E-05	5.84E-05	25.3
-26	2.02E-03		-31.9	22	8.11E-05	1.32E-04	26.6

-25	2.37E-03		-30.6	23	7.55E-05	1.71E-04	27.9
-24	1.89E-03		-29.2	24	5.64E-05	3.37E-04	29.2
-23	1.60E-03		-27.9	25	4.90E-05	3.16E-04	30.6
-22	9.60E-04		-26.6	26	5.12E-05	2.50E-04	31.9
-21	9.25E-04	6.18E-03	-25.3	27	5.09E-05	1.19E-04	33.3
-20	1.16E-03	1.17E-03	-24.0	28	5.31E-05	1.32E-04	34.7
-19	1.46E-03	6.30E-03	-22.7	29	5.02E-05		36.1
-18	1.54E-03	2.99E-03	-21.5	30	5.22E-05		37.6
-17	1.34E-03	1.02E-02	-20.2	31	5.07E-05		39.1
-16	1.10E-03	5.31E-03	-19.0	32	4.99E-05		40.6
-15	6.92E-04	4.66E-03	-17.8	33	4.50E-05		42.2
-14	6.74E-04	9.15E-03	-16.5	34	4.14E-05		43.8
-13	4.68E-04	6.40E-03	-15.3	35	3.60E-05		45.4
-12	7.97E-04	2.00E-03	-14.1	36	3.35E-05		47.1
-11	9.62E-04	3.42E-03	-12.9	37	3.00E-05		48.8
-10	1.04E-03	5.07E-03	-11.7	38	2.81E-05		50.6
-9	1.01E-03	4.42E-03	-10.5	39	2.81E-05		52.5
-8	8.37E-04	1.62E-03	-9.4	40	2.92E-05		54.4
-7	4.68E-04	6.20E-04	-8.2	41	3.31E-05		56.5
-6	4.09E-04	1.53E-03	-7.0	42	3.46E-05		58.7
-5	2.99E-04	3.13E-03	-5.8	43	3.75E-05		61.0
-4	3.72E-04	4.57E-03	-4.7	44	3.72E-05		63.5
-3	7.37E-04	3.98E-03	-3.5	45	3.69E-05		66.2
-2	1.72E-03	1.84E-03	-2.3	46	3.54E-05		69.3
-1	2.82E-03	5.06E-04	-1.2	47	3.76E-05		72.9

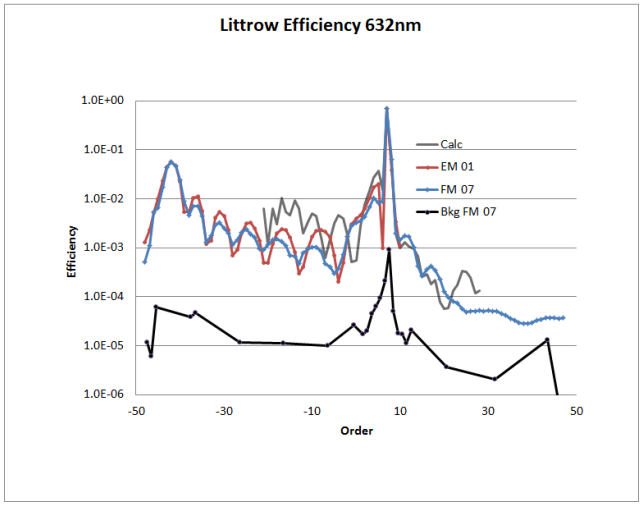

Figure 8. EM-1 and FM-7 measured and calculated grating efficiencies for Littrow configurations at 632.8nm. The peak around order -42 is from the rear facets of the grooves. EM-1 and FM-7 are two replicas of the same master; the red curve is data from St. Cloud State and the blue curve is data from NRL. The black curve is the stray light measured between orders at NRL.

In Figure 8, two independent measurements of two sister replicas of the master grating are seen to be in good agreement. This implies that the groove profile is consistent from master to replica. The calculated efficiencies are in good agreement in the peak orders, and in fair agreement to either side of the peak. Both the measurements and calculations show oscillations in the high order efficiencies, but the calculations are unable to exactly match the measured values. This may be due to the fact that the AFM sample was only 60 microns square and the model profile constructed from this may not contain sufficient detail to fully predict these weak orders. Also presented in Figure 8 are measurements of the stray light between orders made at NRL. The stray light is very low for this ruling, but does peak near the working orders and near the backside orders. This can be understood since the scattering from the groove facets peaks near the specular angle at these two positions.

C. Efficiency calculations versus measured performance for the MIGHTI spectral regions

As reported in Table 1 above, the spectral regions measured by the MIGHTI instrument in the green (557.7nm), red (630.0nm) and near infrared (around 760 nm) correspond to the integer rations of 6, 7, and 8, which allows the use of a low order echelle grating to achieve high efficiency at all these spectral regions.

Figure 9 shows calculated efficiencies in orders 5 – 9 for the MIGHTI gratings using the grating groove profile measured by the AFM. The symbols indicate the measured efficiencies at 557nm and 630nm. While the 557 nm and 630 nm efficiencies are dominated by the n = 8 and 7 orders, respectively, there are small contributions from the n±1 orders. These weak orders are minimized in the final master ruling, but still contribute a wavefront inclined to the main order wavefront. As such, they create a weak, high frequency SHS fringe pattern in addition to the main MIGHTI interferogram. These high frequency fringes are unresolved in the MIGHTI CCD detectors, result in an unmodulated background, and therefore do not affect wind retrievals. The two larger rectangles in Figure 9 indicate the working range of the IR photometer channels (754 nm to 780nm).

Figure 9 illustrates that the calculated and measured efficiencies at 557nm and 630nm are in excellent agreement for the orders shown.

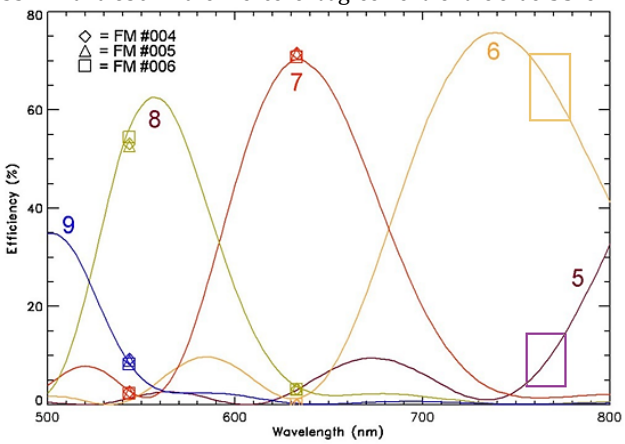

Figure 9. Calculated efficiencies from PCGrate (solid lines) versus measured efficiencies (symbols) MIGHTI gratings in orders 5-9. The two larger rectangles indicate the spectral positions of the IR photometer channels (754 nm to 780nm).

6. FLATNESS OF DIFFRACTED WAVEFRONT

Since it is the interference of two wavefronts that produce the DASH fringes, the plane gratings are specified to produce flat wavefronts to λ/10 or better after four stages of replication. Flatness of the diffracted wavefront was measured with a Zygo interferometer at 633nm. To achieve this, the gratings were set on a precision rotary stage and adjusted until a flat grating edge was perpendicular to the Zygo beam. The grating was then rotated to the Littrow angle and the reflected wavefront observed. Figure 10 is an example of one such profile. All flight quality gratings had a flatness of <0.045 waves RMS at 633nm, including unused portions of groove ends and edges.

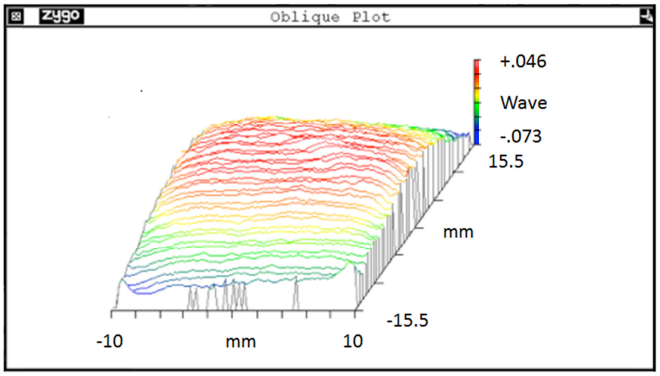

Figure 10. Surface profile map for grating FM-1. The RMS deviation for this grating is 0.024 waves at 633nm; all gratings had an RMS profile deviation of less than 0.045 waves. Piston and tilt errors are removed. These deviations are measured from the 7th order diffracted wavefront and have been divided by two to represent the flatness of the grating.

While it was not possible to precisely control the thickness of the epoxy during replication, the average thickness was 9.0 microns with a standard deviation of 1.2 microns. The epoxy thickness was measured at several points around the margin with a Zygo interference microscope at Light Machinery, Inc. and the gratings were found to be parallel to the substrate with an average deviation of 0.43 arc min, with a standard deviation of 0.40 arc min. These small individual errors (piston, tilt) were then compensated during the interferometer build by slightly adjusting the thickness of the adhesive layers between the grating substrate and the spacer to the field widening prisms (see Fig. 2) while viewing the interference fringes. In addition, the gratings were paired for each interferometer by matching gratings with similar angular offsets between the grating face and substrate plane.

7. ORIENTATION OF GROOVES

The alignment of the grooves started with the manufacture of the grating substrates. The flatness and squareness of the substrate faces had to be suitable for this task (~2 arc min). It was essential to align the plane of dispersion to the edges of the grating blank. This was done with autocollimators and an Ultradex rotary table. This alignment had to be maintained through several generations of grating replication, a challenging task.

In ruling the master, the substrate long side face was used as a reference for the groove direction. In replication, it was used as a reference to maintain this groove orientation on the replica. Interference microscope measurements of the groove tilts relative to an orthogonal face (side of the grating substrate) fell into two groups, one clustered around 13.5 arc min and one clustered around 2.5 arc min. A second orthogonal face (bottom of the substrate) was used as a reference in the interferometer assembly and the resultant direction of the grooves of the two gratings could be made parallel and the wavefront tilts adjusted by adding small tilt corrections while cementing the last grating in place. These small corrections to the grating tip and roll were also made during the assembly process. Once the fringes were straight and of the desired frequency [11], the adhesive was set by exposing it with UV light.

11. ASSEMBLED INTERFEROMETERS

In assembling the gratings on the arms of DASH interferometers, a setup was made in the lab where the interferometer rested on a large optical flat. The flat grating edges were placed against this flat for reference orientation and groove alignment. Light from laboratory sources (HeNe laser 632.8nm, Kr I 558nm, and Ne I 630nm lamps) was used to produce fringes. A reflective Offner mirror assembly and a commercial CCD detector were used to observe the progress of fringe adjustments as they were made. Detailed adjustments to the gratings were made to achieve the desired fringe frequencies [11] at the above wavelengths. When straight fringes and a stable alignment was achieved, minute drops of UV setting adhesive were introduced to wick into the seams between the gratings and spacers, and were hardened by overnight exposure to UV light. Figure 11 is a photo of an assembled interferometer.

8. CONCLUSIONS

A new master echelle grating and eight sister replica gratings of outstanding performance have been produced for the MIGHTI instrument on ICON. Six of these gratings have been assembled into three flight interferometers and two into an engineering model. Two cosmetically less perfect gratings are flight spares and have been the subject of some of the testing reported here. The gratings have near theoretical performance, and operate in 6th, 7th, and 8th orders at 760, 630, and 557nm, and the flatness of the gratings (~λ/20) is sufficient for interferometry at these wavelengths. Efficient groove shapes and gold coatings give them highest efficiency (>70%) at 630nm, optimized for measurements of the faint atmospheric O I 630nm line. Laser measurements of the grating efficiency in many orders have been made in both the Littrow configuration and in the MIGHTI working configuration. A groove profile has been obtained from AFM measurements and used to calculate grating efficiencies with the PCGrate code. With a small empirical adjustment to the groove angle, PCGrate efficiency calculations were in good agreement with experimental measurements.

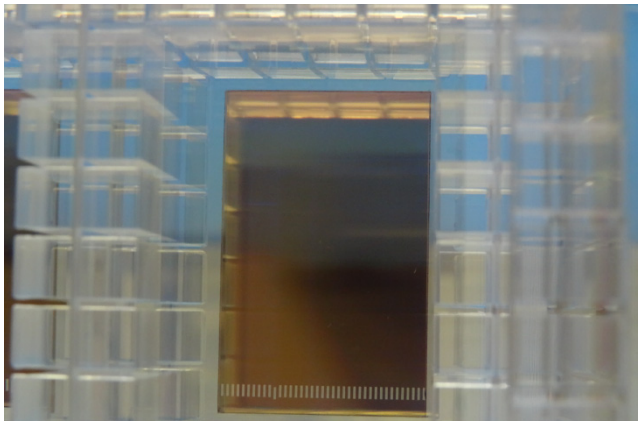

Figure 11. View looking into the entrance aperture of a MIGHTI interferometer after assembly. The two gratings are superimposed in this view. The rectangular blocks are precision spacers that maintain optical gaps while allowing for some thermal mismatch between different optical glasses [11]. A row of laser inscribed fiducial marks is seen on the lower edge of the right grating. Since the fringe localization plane is at the grating face, these marks will also be in focus at the detector and allow tracking of grating image movements due to thermal distortion etc. [16].

Funding Information. The ICON mission is supported by NASA's Explorers Program through contracts NNG12FA45C and NNG12FA42I.

Acknowledgment. We thank Dr. Leonid Goray for assistance with the PCGrate code calculations of the grating efficiency.

References

1. Englert, C.R., Harlander, J. M., Brown, C. M., Marr, K. D., Miller, I. M., Stump, J. E., Hancock, J., Peterson, J., Kumler, J., Morrow, W. H., Mooney, T., Ellie, S., Mende, S. B., Harris, S. E., Stevens, M. H., Makela, J. J., Harding, B. J., Immel, T. J., "Michelson Interferometer for Global High-resolution Thermospheric Imaging (MIGHTI): Instrument Design and Calibration," Space Sciences Reviews (2017) Accepted.

2. Sheese P. E., Llewellyn, E. J., Gattinger, R. L., Bourassa, A. E., Degenstein, D. A., Lloyd N. D., McDade I. C., "Temperatures in the upper mesosphere and lower thermosphere from OSIRIS observations of O_2 A-band emission spectra," Can. J. Phys., 88, 919-925 (2010).

3. Christensen, A. B., Yee, J.-H., Bishop, R. L., Budzien, S. A., Hecht, J.H., Sivjee, G., Stephan, A. W., **"**Observations of molecular oxygen Atmospheric band emission in the thermosphere using the near infrared spectrometer on the ISS/RAIDS experiment," J. Geophys. Res., 117, doi:10.1029/2011JA016838 (2012).

4. Shepherd, G. G., Thuillier G., Cho, Y.-M., Duboin, M.-L., Evans, W. F. J., Gault, W. A., Hersom, C., Kendall, D. J. W., Lathuillère, C., Lowe, R. P., McDade, I. C., Rochon, Y. J., Shepherd, M. G., Solheim, B. H., Wang, D.-Y. , Ward W. E., "The Wind Imaging Interferometer (WINDII) on the Upper Atmosphere Research Satellite: A 20 Year perspective, Reviews of Geophysics," 50, **RG2007**, 2012RG000390 (2012).

5. Harlander, J. M., Reynolds, R. J., Roesler F. L., "Spatial Heterodyne Spectroscopy for the Exploration of Diffuse Interstellar Emission Lines at Far-Ultraviolet Wavelengths," Astrophys. J. **396**, 730 (1992).

6. Englert, C. R., Harlander, J.M., Babcock, D.D., Stevens, M.H., Siskind, D.E., "Doppler Asymmetric Spatial Heterodyne Spectroscopy (DASH): An innovative concept for measuring winds in planetary atmospheres," Proc. of SPIE, 6303 63030T (2006).

7. Englert, C. R., Babcock, D. D., Harlander J. M., "Doppler Asymmetric Spatial Heterodyne Spectroscopy (DASH): Concept and Experimental Demonstration," Appl. Opt., **46**, 7297 (2007).

8. Englert, C. R., Harlander, J.M., Emmert, J.T., Babcock, D.D., Roesler F.L., "Initial thermospheric wind measurements using a ground-based DASH interferometer," Optics Express, **18**, 27416-27430 (2010).

9. Englert C.R., Harlander, J. M., Brown, C. M., Meriwether, J. W., Makela, J. J., Castelaz, M., Emmert, J.T., Drob, D.P., Marr K.D., "Coincident Thermospheric Wind Measurements using ground-based Doppler Asymmetric Spatial Heterodyne (DASH) and Fabry-Perot instruments," Journal of Atmospheric and Solar-Terrestrial Physics, **86**, 92-98, doi:10.1016/j.jastp.2012.07.002 (2012).

10. Englert , C. R., Stevens., M. H., Siskind, D. E., Harlander J. M., Roesler, F. L. , "Spatial Heterodyne Imager for Mesospheric Radicals on STPSat-1," J. Geophys. Res., **115**, D20306, doi:10.1029/2010JD014398 (2010).

11. Harlander, J. M., Englert, C. R., Brown, C. M., Marr, K. D., Miller, I. J., Zastera, V., Bach, B. W., Mende, S. B., "Michelson Interferometer for Global High-resolution Thermospheric Imaging (MIGHTI): Monolithic Interferometer Design and Test," Space Sciences Reviews (2017) Accepted.

12. Goray, L., International Intellectual Group Inc., P.O. Box 335, Penfield, N.Y. 14526, http://www.pcgrate.com (2015).

13. Goray, L. I. and Seely, J. F., "Efficiencies of Master, Replica, and Multilayer Gratings for the Soft X-Ray - Extreme Ultraviolet Range: Modeling Based on the Modified Integral Method and Comparisons with Measurements," Appl. Opt. **41**, 1434 (2002).

14. Seely, J. F. J. F. Seely, C. M. Brown, D.L. Windt, S. Donguy, and B. Kjornrattanawanich**,** "Normal Incidence Efficiencies of Multilayer-Coated Laminar Gratings for the Extreme-Ultraviolet Imaging Spectrometer (EIS) on the Solar-B Mission." Appl. Opt. **43**, 1463 (2004).

15. Palik, E. D. ed., *Handbook of Optical Constants of Solids*, Academic Press, New York (1985).

16. Marr, K. D., Englert, C. R.,Harlander, J.M., Miller, K. W., "Thermal sensitivity of DASH interferometers: the role of thermal effects during the calibration of an Echelle DASH interferometer." Appl. Opt., **52**, 8082 (2013).